Scalable Three-Dimensional Photobioelectrodes Made of Reduced Graphene Oxide Combined with Photosystem I

Sascha Morlock, Senthil K. Subramanian, Athina Zouni, and Fred Lisdat

Scalable 3D Photobioelectrodes made of Reduced Graphene Oxide combined with Photosystem I

Sascha Morlock[a,b], Senthil K. Subramanian[b], Athina Zouni[b], Fred Lisdat[a]**

[a] Biosystems Technology, Institute of Life Sciences and Biomedical Technologies, Technical University of Applied Sciences Wildau, Hochschulring 1, 15745 Wildau, Germany

[b] Biophysics of Photosynthesis, Institute for Biology, Humboldt University of Berlin, Philippstraße 13, 10115 Berlin, Germany

* Corresponding authors

KEYWORDS Biophotovoltaics, reduced graphene oxide (rGO), scalable template process, spin-coating, 3D electrode structure, carbon material.

Abstract

Photobioelectrodes represent one of the examples where artificial materials are combined with biological entities to undertake semi-artificial photosynthesis. Here, an approach is described that uses reduced graphene oxide (rGO) as electrode material. This classical 2D material is used to construct a three-dimensional structure by a template-based approach combined with a simple spin-coating process during preparation. Inspired by this novel material and photosystem I (PSI),

a biophotovoltaic electrode is being designed and investigated. Both, direct electron transfer to PSI and mediated electron transfer via cytochrome *c* from horse heart as redox protein can be confirmed. Electrode preparation and protein immobilization have been optimized. The performance can be upscaled by adjusting the thickness of the 3D electrode using different numbers of spin-coating steps during preparation. Thus, photocurrents up to 14 µA/cm² are measured for 12 spin-coated layers rGO corresponding to a turnover frequency of 30 e^- PSI^{-1} s^{-1} and external quantum efficiency (EQE) of 0.07 % at a thickness of about 15 µm. Operational stability has been analyzed for several days. Particularly the performance at low illumination intensities is very promising (1.39 µA/cm^2 at 0.1 mW/cm^2 and -0.15V vs. Ag/AgCl; EQE 6.8 %).

1. Introduction

In order to exploit solar energy, nature uses photosynthesis – a process that is at least about three billion years old. [1] For the conversion of sunlight to excited electronic states, higher plants, algae, and cyanobacteria use a multistep process based on two photoactive pigment protein complexes called photosystem I and II (PSI and PSII). At +1.2 V vs standard hydrogen electrode (SHE), the cationic radical $P680^{+*}$ in PSII has the highest natural oxidation potential known to date, at which the splitting of water takes place. [2–4] On the other hand, the $P700^*$ in PSI is the strongest reductant identified in nature at a potential of -1.3V (vs SHE). [3–5] Due to internal electron transfer steps, the electrons lose some energy and exit PSI at -0.58 V (vs SHE). This energy is sufficient to reduce ferredoxin and subsequently $NADP^+$. [4]

The increased biotechnological application of PSI is based on the high stability of the trimer multi-pigment protein complex from *Thermosynechococcus elongatus* even under high light conditions. Furthermore, in PSI light is converted into charge carriers with an internal quantum

efficiency of almost 100%. In contrast, even under moderate light conditions, PSII is less suitable for electrochemical applications due to its instability caused by the inability to repair and re-assemble PSII rapidly in an *ex vivo* situation. This process primarily involves the replacement of the D1 core subunit that especially prone to oxidative damage, which is caused by the light-driven oxidation of water. [6,7]

Humanity can utilize the competence of nature for sunlight conversion in biohybrid photovoltaic devices. In these systems, artificial electrode materials are combined with photoactive protein complexes, like PSI, [8–11] PSII [12–14], or bacterial reaction centers. [15–17] Alternatively, thylakoid membranes [18–20] or whole cells [21–23] are used for biohybrid electric current production. In a more advanced step, additionally, the production of valuable chemicals is implemented. [24,25] Furthermore, biophotovoltaics, as photobioelectrodes are called alternatively, can optionally be used as photobiosensors. [19,26]

One of the challenges in the field of bioelectrochemistry is the electrical interaction of man-made material and biological compounds. To this end, three different routes can be distinguished: direct, wired, and mediated electron transfer. [27] In biophotovoltaics successful examples for all these electron transfer mechanisms can be found in the literature. PSI has been connected directly to graphene. [28,29] It has been entrapped in poly-benzylviologen or polyaniline for wired electron transfer. [30,31] Mediated electron transfer was achieved via redox polymers, [12,16] small redox molecules, [32,33] as well as different cytochromes. [9,34,35]

In recent years, significant efforts have been devoted to increasing the efficiency of photobioelectrodes based on PSI. [5,36] These electrodes can be constructed on different flat 2D electrodes. [11,33,35,37] In order to increase the photocurrent per geometrical area, multiple three-dimensional architectures have been developed: multilayers, [30,38,39] hydrogels, [16,40,41] and 3D

electrode setups. [14,34,42] Different materials proved to be adaptable to biophotovoltaics including gold, [11,43] indium tin oxide (ITO), [14,30,34] antimony tin oxide, [44] and TiO_2. [45,46] Electrodes based on carbon materials, such as carbon nanotubes, [32] fullerenes, [47] graphene, [28,29,35,48] and reduced graphene oxide (rGO),[33] have the inherent advantage that they are free of heavy metal elements.

Due to its properties, in particular, high conductivity and mechanical strength at low weight, graphene has gained an accretive interest in materials chemistry. [49,50] Graphene was first synthesized in 2004. [51] Within years, many different synthesis routes for graphene have been developed, e. g. mechanical [52] as well as liquid-phase exfoliation, [52] chemical vapor deposition,[52] and synthesis on SiC. [53] Nevertheless, merely the reduction of graphene oxide results in high yields at low cost in an extendable process. [54] Graphene oxide can be reduced by many different methods including electrochemical, [55] thermal, [56] and chemical treatment. [57] Three-dimensional graphene-based materials are just a recent development that combines the advantages of both, graphene and 3D architectures. [58]

The goal of the present publication is the preparation of a scalable three-dimensional photobioelectrode based on rGO and PSI. Graphene has already been shown to be useful in coupling PSI as stated above. [28,29,35,48] In a 2D setup rGO has also successfully been coupled to PSI. [33] Furthermore, a biophotovoltaic system combining 3D rGO and PSII has been achieved. [14] However, a 3D rGO electrode is a novelty for PSI.

2. Experimental

2.1. Materials and Chemicals

The following chemicals have been purchased from Sigma Aldrich, Germany: graphene oxide suspension in water (4 mg/mL) (GO), latex beads suspension in water (3 µm mean size; 10%)

(LB), aqueous ammonia solution (28%), hydrazine solution in water (35%), sulfuric acid (95-98%), 5-hexenoic acid (98%), and cytochrome *c* (horse heart; ≥95%) (cyt *c*). Acetone (≥99.8%), 2-propanol (≥99.7%), and potassium hydroxide (>85%) have been supplied by VWR, Germany. Roth, Germany, provided potassium chloride (>99%), orthophosphoric acid (85%), and potassium dihydrogen phosphate. Potassium hydrogen phosphate (>99%) has been purchased from Fluka, Germany, and 4,4'-bipyridine (99.9%) from Riedel-de Haën, Germany.

For all experiments, ultrapure water has been used, which was received by an SG Ultra Clear UV plus, Netherlands. Potassium phosphate buffer (PPB) pH 7 was prepared by mixing the required amounts of potassium dihydrogen phosphate and potassium hydrogen phosphate in water. The pH was controlled by a pH electrode from Sartorius, Germany.

2.2. Isolation and Purification of Photosystem I

Cultivation of *Thermosynechococcus elongatus* and extraction of proteins from thylakoid membranes were performed according to Kern et al.. [59] PSI was purified from detergent-solubilized membrane proteins by using two ion-exchange columns as previously described. [60] The trimeric PSI from the second column was concentrated using an Amicon stirred filtration cell on a Biomax 100 membrane (Millipore, Germany). The PSI trimer was crystallized by slowly diluting against buffer A (5 mM MES-NaOH, pH 6.0, and 0.02% n-dodecyl-β-D-maltoside (β-DM) at 4 °C) as previously described. [60] The crystals were washed in buffer A, solubilized in buffer A containing 150 mM $MgSO_4$ and crystallized again as mentioned before. The re-solubilization and crystallization steps were repeated at least three times. The concentration of PSI-bound chlorophyll a was determined in buffer A containing 150 mM $MgSO_4$ by ε_{680} = 57.1 mM^{-1} cm^{-1} and the concentration of reaction center (P700) was determined by ε_{680} = 5.5 mM^{-1} cm^{-1}. [61] The purity was

assessed by Blue native-polyacrylamide gel electrophoresis and dynamic light scattering. [62] The photochemical activity of purified PSI trimer was assessed with cyt *c* as an electron donor using a Clark electrode (Hansatech) as previously reported. [60]

For the preparation of the photobioelectrodes, the PSI crystals have been washed several times with 5 mM PPB (pH 7). Here the suspensions were centrifuged at 1,000 rpm (93 *rcf*) at 4 °C for 5 min. The supernatant was discarded, and this washing process was repeated until a clear supernatant was observed. After approximately 5 washing steps, the crystal pellet was solubilized in 100 mM PPB (pH 7). UV/VIS spectroscopy was used to set the concentration of the PSI trimer to 30 µM.

2.3. Preparation of 3D rGO Electrodes

Glassy carbon electrode chips (GCE) of about 12 x 8 mm were cleaned in an ultrasonication bath for 15 min each in water, acetone, and 2-propanol. The 3D structure was fabricated by a spin-coating process inspired by a procedure for 3D ITO. [34] The solution for spin-coating was prepared as follows: 50 µL LB (10 wt% in water), and 83.3 µL GO suspension (0.4 wt% in water) were dispersed in 1 mL isopropyl alcohol via ultrasonication. This suspension was centrifuged at 16,400 rpm (25,000 *rcf*) for 8 min at 4 °C. The supernatant was discarded, and the pellet was resuspended in another 1 mL 2-propanol by ultrasonication. The centrifugation step was repeated as above, and the supernatant was discarded again. The pellet was resuspended by ultrasonication in 95 µL 2-propanol to result in a total final volume of 100 µL.

Subsequently, 8 µL of this suspension was dropped on a GCE that rotated at a spin-coater at 4800 rpm. This was repeated 3 to 15 times to produce 3D structures of different thicknesses. After spin-coating, the obtained structure was placed in acetone at room temperature overnight to

remove the LB. To eliminate polystyrene residues, a second incubation in acetone was used the following day for 30 min. Acetone was removed from the structure by three times incubation in water for a total of at least 30 min. For the reduction of GO, a known process from literature was adapted to be suitable for the GCE based electrodes at hand. [63] Each electrode was placed in a tube filled with 1 mL of an aqueous solution containing 7 µL ammonia (28%) and 1 µL hydrazine (35%) solutions. The reduction of GO was performed at 99 °C and 1,400 rpm for one hour in a Thermomixer comfort (Eppendorf, Germany). The electrode was cleaned by incubation in the water at least three times for a total of 30 min. Finally, the finished electrode was incubated in ethanol and dried in air. The electrodes were either stored in air or modified overnight as described in chapter 2.4.

2.4. Modification of the 3D rGO Electrodes

Different methods for surface modification have been used:

A) Electrochemical surface modification was conducted in 0.5 M sulfuric acid. Thereby cyclic voltammetry was carried out in the range of -0.6 to 1.4 V vs. Ag/AgCl for 20 min at a scan rate of 100 mV/s. Later, the 3D rGO electrodes were thoroughly cleaned by placing them in water for three minutes.

B) Acidic groups have been introduced by the following procedure: The 3D rGO electrodes were placed in a 0.5 mM ethanolic solution of 5-hexenoic acid. Meanwhile, they were illuminated by UV light at a wavelength of 254 nm for 16 h. Subsequently, they were dipped first in ethanol and then in water.

C) The 3D rGO electrodes were non-covalently modified by bipyridine (bipy). Thereto, the electrodes were placed into a 5 mM aqueous bipy solution. After incubation at room temperature overnight, unbound bipy residues were removed carefully by several dipping steps into the water.

All surface modifications were done immediately before protein immobilization.

2.5. Preparation of the Photobioelectrodes

Incubation with biomolecules was always performed the day after the reduction of GO and immediately before measurement. To adapt to the different available surface areas for different thicknesses of the prepared electrodes, always 1 µL of the protein solution was used per spin-coated layer. The incubation time was usually 3 min except for the investigations described in chapter 3.2. For the variations in immobilization strategies (chapt. 3.2) and surface modifications (chapt. 3.3), solutions of 30 µM trimeric PSI, as well as 1 mM cyt *c*, were used. The remaining measurements (chapt. 3.4 to 3.6) were conducted with a 1:1 mixture of both protein solutions (15 µM PSI and 500 µM cyt *c*). After incubation, excessive biomolecules were carefully removed by dipping the electrode into 5 mM PPB (pH 7). During measurement, the electrode area in interaction with the electrolyte was confined by using an O-ring in a self-made cell to a surface of 0.125 cm^2.

2.6. Determination of the Coverage of Biomolecules

The cyt *c* loading was calculated using cyclic voltammetry. A cyclic voltammogram (CV) was recorded after the photoelectrochemical characterization of the electrodes at a scan rate of 100 mV/s in the range from -500 to 500 mV vs. Ag/AgCl in 5 mM PPB pH 7. Five cycles were

performed to allow for stabilization. The cyt *c* loading was determined by analyzing the faradaic current in the CV during oxidation in the range of about 0 to 200 mV.

The number of PSI molecules was determined via UV/VIS spectroscopy. In order to reliably determine the PSI loading on the electrode, the following procedure was conducted inspired by a protocol described in the literature. [14] 3D rGO structure was prepared on fluorine-doped tin oxide (FTO) instead of GCE because it is easier to remove it later. Every other step in the preparation remained unchanged. Instead of a photocurrent measurement in the measurement cell these electrodes were placed in 5 mM PPB (pH 7) for 25 min. Afterwards they were dried under air. Next all the 3D rGO (that was prepared and incubated with the PSI cyt *c* mixture) was scratched from the surface into a microcentrifuge tube. 160 µL 80% acetone was added for 1 h to extract the chlorophyll. Then the tube was centrifuged at 1,000 rpm (93 rcf) at 4 °C for 2 min. UV/VIS spectroscopy was performed in the range of 350 to 750 nm at a rate of 600 nm per min. PSI coverage was calculated using a modified formula of Porra. [64]

2.7. Electrochemical and Photoelectrochemical measurements

All electrochemical measurements were repeated with at least 3 electrodes to avoid coincidence. The standard deviation of 3 or 4 (where applicable) measurements was used to depict the error bars in the graphics. A three-electrode setup was used consisting of the novel 3D rGO electrode as a working electrode, a platinum wire as a counter electrode and an Ag/AgCl, 3M KCl reference electrode (DRIREF-2SH by World Precision Instruments, USA).

All photoelectrochemical experiments have been performed by a Zennium PP211, a photoelectrochemical workstation by Zahner (Germany). A white light source was used at a power of 100 mW/cm², spectrum (see Figure S1). Photocurrents were measured at a potential of -0.15 V

vs Ag/AgCl. For chopped-light voltammetry, the applied potential was varied at a rate of 2 mV/s from 0.2 to -0.5 V vs Ag/AgCl. Photo action spectroscopy was performed with a Polychrome V by FEI, USA.

The turnover frequency (TOF) was calculated the following: The measured photocurrents were converted into excited electrons per second. This number was divided by the number of PSI trimers that was measured as described in chapter 2.6.

For electrochemical characterization of the basic electrode, cyclic voltammetry was performed on a CH Instruments Electrochemical Analyzer, USA. UV/VIS spectroscopy was undertaken on an Evolution 300 UV-VIS spectrometer by Thermo Scientific, Germany. For spin-coating a KLM Spin-Coater SCC by Schaefer Technologie GmbH, Germany was used. Scanning electron microscopy was performed by the scanning electron microscope JSM-6510 by JEOL, Japan.

3. Results and Discussion

3.1. Characterization of the Electrode Material

Due to its electrochemical properties, reduced graphene oxide (rGO) has been selected as the electrode material for novel biophotovoltaics in this study. To ensure a high photocurrent magnitude a 3D structure has been fabricated. Thus, a template-based approach using polymeric beads and graphene oxide has been applied. After spin-coating a different number of layers, the beads are dissolved by acetone and subsequently, a reduction process exploiting hydrazine is followed. As a new electrode material has been prepared, it is important to characterize this material before its use in photobioelectrodes. The 3D structure has been examined by scanning electron microscopy (SEM) and the electrochemical behavior of the 3D rGO has been evaluated with cyclic voltammetry (CV). SEM images of an rGO electrode prepared with 12 spin coating

steps in the preparation are shown in Figure 1. A 3D architecture can be seen with pores and holes that enable the biomolecules to penetrate the electrode structure (Figure 1A). The side view in Figure 1B clearly illustrates that the assembly of multiple layers of spheres has been successful. At a higher magnification of 10,000, the rGO flake structure can also be seen (Figure 1C).

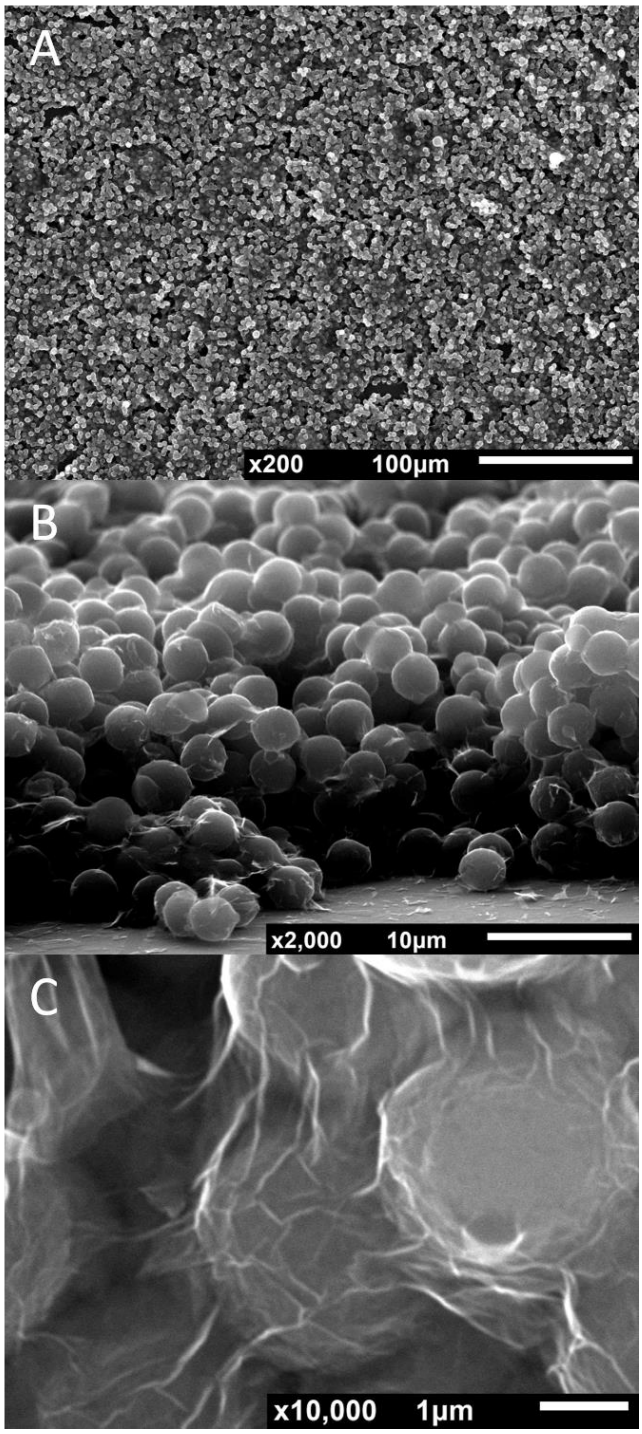

Figure 1. SEM images of an electrode consisting of 12 layers of rGO at different magnifications. (A), (C) top view. (B) side view at an angle of 80°.

CV has been first performed in potassium phosphate buffer (pH 7) (Figure 2). Compared to the CV of the underlying GCE significantly higher charging currents have been obtained. A direct area comparison cannot be made since the capacitance of the different carbon surfaces is not equal, particularly since high specific capacitances are reported for rGO. [65] However, the 3D structure leads to a larger accessible surface per geometrical area. No faradaic currents are prominent in the CV meaning that there are no electrochemically active species on the surface. Second, the surface has been tested for electrochemical activity. Here, ferrocene carboxylic acid has been applied in solution and a quasi-reversible behavior can be observed at this interface.

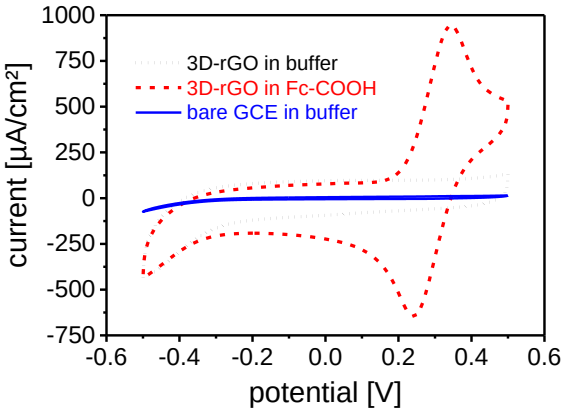

Figure 2. Cyclic voltammograms of the basic 3D rGO electrode measured at 100 mV/s in 100 mM PPB (pH 7) (black dots) as well as in buffer + 5 mM ferrocene carboxylic acid (red dashes) and CV of a bare GCE in 100 mM PPB (pH 7) (blue line). Potential -0.5 to 0.5 V vs. Ag/AgCl.

3.2. Protein Immobilization

As illustrated in Figure 3, two different strategies of establishing communication between PSI and the electrode have been studied. First, direct communication of PSI with the rGO electrode (DET) which is based on studies from graphene-based electrodes, [28,29] and second, a mediated electron transfer via the redox protein cyt *c* (MET) which is based on studies demonstrating the usefulness of the non-natural reaction partner of PSI in interacting with both the electrode and PSI. [32,47] Consequently, different approaches have been investigated for the immobilization of these proteins. Here, one relies on the spontaneous adsorption of the proteins from an aqueous solution. For these investigations, electrodes with a thickness of the 3D rGO of about 8 µm have been applied (6 spin-coating steps in preparation).

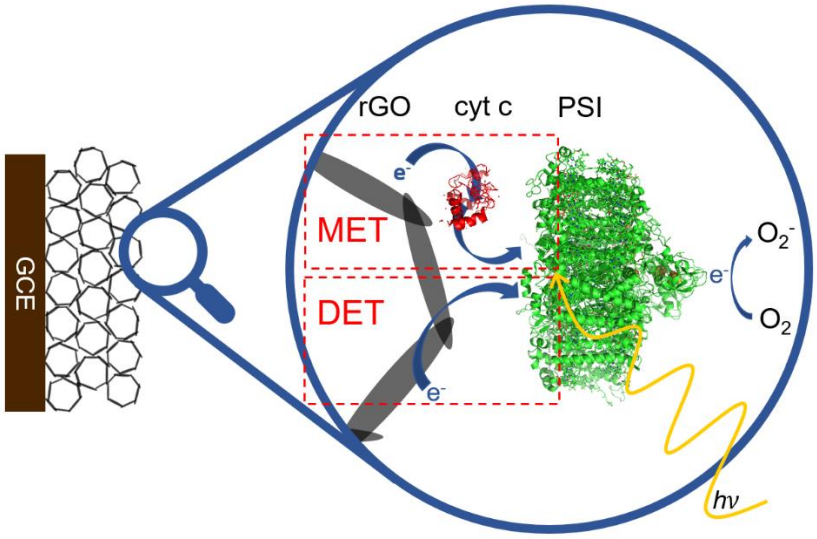

Figure 3. Illustration of the two evaluated working principles of photobioelectrodes. The transfer of an electron from the artificial electrode material to the luminal side of PSI can either be mediated via cyt *c* (MET) or directly (DET). In both cases, an electron is excited in PSI by light and transferred finally to oxygen at the stromal side of the biomolecule.

First, chopped-light voltammetry is used to evaluate the photoelectrochemical behavior of the photobioelectrode. In Figure 4A two measurements for an electrode incubated solely with PSI for 3 min as well as another electrode treated with PSI and cyt *c* for 3 min each are given. The measurements show that the prepared 3D electrodes are suited for the construction of biophotovoltaic systems. The photocurrent magnitude benefits from the use of the redox protein as an immobilized shuttle. Besides, the onset potential of the cathodic photocurrent is about

-0.03 V vs. Ag/AgCl for the reaction of PSI alone and 0.07 V vs. Ag/AgCl for the reaction of PSI via cyt *c*. That means that the overpotential for electron flow from 3D rGO to PSI can be reduced by 100 mV when using MET via cyt *c*.

For a better analysis of the photocurrent behavior, measurements at a constant potential have been performed in a next step. A potential of -0.15 V vs. Ag/AgCl is selected here and the photobioelectrodes are illuminated with an intensity of 100 mW/cm² for 30 s. Foremost the PSI-rGO system has been evaluated. Therefore, the electrodes are incubated with PSI solution for 3 and 60 min, respectively. Photocurrents of 0.48 ± 0.19 or 0.14 ± 0.02 µA/cm², in the latter case, verify that DET between the rGO surface and PSI takes place. Figure 4B also illustrates the kinetic behavior which indicates a slow component in establishing the photocurrent response after the start of the illumination when only PSI is used.

A more than ten-fold increase of the photocurrent magnitude can be achieved via MET by the addition of cyt *c* as a mediator. Note that in this case both proteins are studied immobilized on the rGO. Here, photocurrents up to 6.35 ± 2.11 µA/cm² are measured for electrodes that have been prepared by 3 min incubations with PSI and cyt *c*. The kinetic analysis shows that the photocurrent of electrodes with cyt *c* reaches a steady-state level much faster than that without the redox protein (inset Figure 4B).

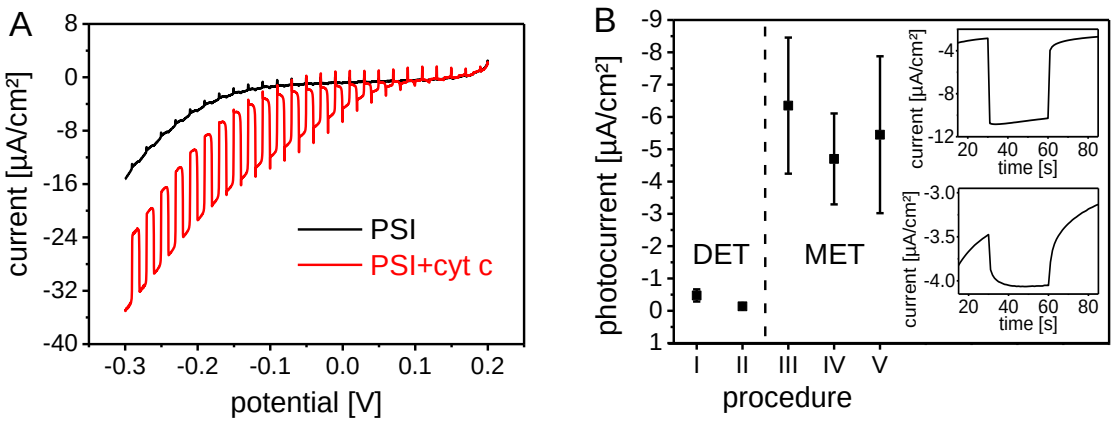

Figure 4. (A) Chopped-light voltammetry of two photobioelectrodes at a scan rate of 2 mV/s. The black curve shows the 3D rGO electrode with PSI alone whereas the red curve the electrode with

PSI and cyt *c* (B) Results of a test series, where different immobilization methods for the involved proteins have been tested; c_{psI} = 30 µM, 100 µM PPB pH 7; $c_{cyt\ c}$ = 1 mM, 5 mM PPB pH 7. (I) 3 min PSI; (II) 60 min PSI; (III) 3 min PSI and cyt *c* each; (IV) 60 min PSI, 3 min cyt *c*; (V) 60 min PSI and cyt *c* each. Insets: Examples of the photocurrent measurements for procedures I (below) and III (above). Error bars represent the standard deviation of 3-4 measured electrodes.

These measurements have also been used to investigate the influence of the time for protein immobilization on the photocurrent output. Here, a period from 3 to 60 min has been studied. As exemplified in Figure 4B there is no strong tendency with different time frames for the protein-electrode contact. Therefore, in the following short protein incubation times have been applied.

In consequence, it can be stated that a DET of immobilized PSI with the newly prepared electrode material is feasible. Yet, it results only in small current densities and rather low onset potentials. Electrodes with cyt *c* and thus, based on a MET principle provide larger photocurrents and an onset potential which is just above 0 V vs. Ag/AgCl and thus, corresponds to the electrochemical reaction of cyt *c*.

3.3. Surface Modification

The first test series in chapter 3.2 indicates that functional electrodes can be constructed with both proteins immobilized on rGO. In the following, it has been tested whether a surface modification can be used to improve the photocurrent behavior. For this purpose, again rGO electrodes prepared with 6 spin coating steps are used. To enhance the hydrophilicity in a first approach, 3D rGO has been cycled in 0.5 M sulfuric acid before protein immobilization. As can be seen in Figure 5, the modification leads to an improvement of the mean photocurrent value for

the direct interaction of PSI with the electrode (B1) compared to the unmodified rGO (A1). For the system with both proteins, only a slight increase relative to the non-treated surface (A2) can be found which is counterbalanced by a large variation in performance among the prepared electrodes (B2).

One can expect that this CV treatment induces a variety of polar groups on rGO. A more controlled procedure solely introducing carboxylic functions has been conducted in the next approach. This is based on the immobilization of alkenes on carbon surfaces. For example, Baker et al. have increased the electrochemical interaction of cyt *c* and carbon nanofibers significantly by this method [66]. Therefore, hexenoic acid has been applied to rGO and activated by UV light. Again, the DET of PSI on such a surface can be improved – although it remains small (Figure 5C1). But the mediated systems show a similar performance as without the pretreatment (C2).

As the third modification strategy, an incubation in an aqueous bipyridine (bipy) solution has been chosen since these molecules cannot only bind to carbon but are also able to facilitate electron transfer to cyt *c* [28,29]. While there is no measurable effect for the direct PSI-rGO interaction (Figure 5: D1 compared to A1), there is a slight increase in photocurrent for the cyt *c*-based system (D2). However, also here the large variations among different electrodes counterbalance to a certain extent. An additional argument for the usage of this modification agent, however, may come from the potential dependent photocurrent analysis. Chopped-light voltammetry proves that the onset-potential for the cathodic photocurrent generation shifts slightly to higher potentials (from 0.07 V to 0.11 V vs. Ag/AgCl (see Figure S2)) and thus, the overpotential is reduced. Hence, for all further electrode constructions, a bipy-treatment is performed.

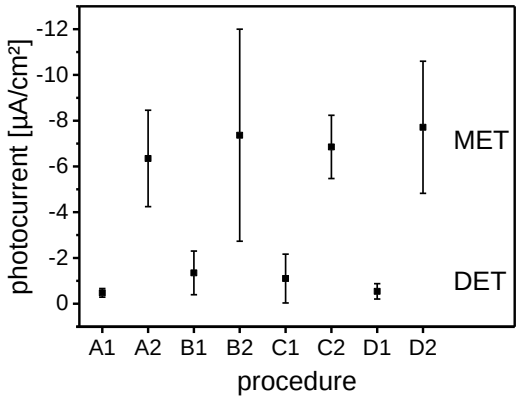

Figure 5. Photocurrent of PSI-based photobioelectrodes treated with different surface modification techniques before protein immobilization. (1) DET of PSI without cyt *c*; (2) MET of PSI with cyt *c*. Modifications: (A) No surface modification; (B) cyclic voltammetry in sulfuric acid; (C) UV treatment with hexenoic acid; (D) incubation in bipyridine solution. Error bars refer to the standard deviation of 3-4 measurements.

3.4. Optimization of the Incubation Process

The surface modification with bipyridine leads to the highest photocurrents as can be seen in Figure 5. However, the standard deviation is relatively high. To validate the observed increased photocurrent, the incubation process has been optimized. For all the further evaluations, only MET has been considered. As an alternative immobilization approach, a mixture of PSI and cyt *c* has been applied. Thereby, indeed a more precise protein coating has been achieved. As measurements prove (see Figure S3) the relative standard deviation can be reduced due to that approach by a factor of 2.8. Furthermore, the photocurrent is slightly increased.

3.5. Scalability

To enhance the photocurrent per geometrical area, one can easily increase the thickness of the 3D material – provided the preparation method is scalable. To effectively achieve better performances, the following conditions need to be fulfilled:

(i) When multiple deposition steps are added, the thickness of the electrode has to increase accordingly. This also means that the structure must be mechanically stable.

(ii) Even when thicker structures are prepared the conductivity should not go down.

(iii) For effective light interaction, the transparency of the electrode structure has to be maintained to a certain degree.

These different criteria have been evaluated for different thicknesses of the 3D rGO by SEM, CV, and UV/VIS spectroscopy. To this end, 3D rGO electrodes are prepared by applying 3, 6, 9, 12, and 15 spin-coating steps during preparation and characterized.

For the determination of the thickness of the structure, SEM images at an angle of 80° are taken and an electrode with the respective numbers of spin-coated steps has been analyzed at 7 different points. The mean thickness value and the standard deviation are determined which can be seen in Figure 6A. It is obvious that the build-up of thicker structures is indeed possible and results in mechanically stable 3D electrodes. The thickness increases linearly up to 15 spin-coating steps.

Subsequently, CV has been used to determine the electrochemically accessible surface area. The capacitive currents are determined for at least 3 electrodes and compared at a potential of 200 mV vs Ag/AgCl. Again, a clear linear correlation to the number of deposition steps can be seen in Figure 6A.

For the UV/VIS measurements, 3D rGO electrodes have been prepared on FTO instead of GCE for transparency reasons. Apart from this variation, other parameters remain unchanged in the process. A minimum of 3 electrodes has been fabricated for each number of spin-coating steps.

The absorbance has been analyzed at 680 nm (wavelength of high absorbance of PSI). A linear increase in absorbance with the number of spin-coating steps has been observed. This also means, however, that transmission is diminished to less than 1.4 % when 15 deposition steps have been reached.

These results demonstrate that the chosen preparation process is highly scalable for the basic electrode properties. This provides a solid basis for the construction of a whole biophotovoltaic system to analyze the scalability with respect to functionality.

Figure 6B illustrates the photocurrent behavior for photobioelectrodes prepared with varying deposition steps in preparation and thus, different thicknesses. The results clearly show that all systems can generate photocurrents. The magnitude of this photoresponse can be increased significantly by the upscaling of the 3D rGO. For electrodes prepared with up to 12 spin-coating steps, the photocurrent gain is almost linear, thus values up to 13.7 ± 1.4 μA/cm² have been achieved at -0.15V vs Ag/AgCl.

At higher thickness, no significant increase in photocurrent has been observed. To analyze limiting factors, the loading of the two proteins has been studied. As Figure 6C shows a linear raise of the PSI and cyt *c* coverage, rather unhindered access of the proteins to the 3D rGO surface can be assumed.

This means that thicker electrodes also have the benefit of a higher surface, which is still accessible for both proteins – PSI as the photoactive component and cyt *c* as the component responsible for efficient wiring of PSI to the electrode surface. However, one has to note that the transparency at higher thicknesses is becoming relatively low, i. e. only a few percent of the initial intensity. Despite the larger surface and higher protein loading, the diminished light interactions

seem to be the main reason for the limitation in photocurrent generation above 12 spin-coated layers.

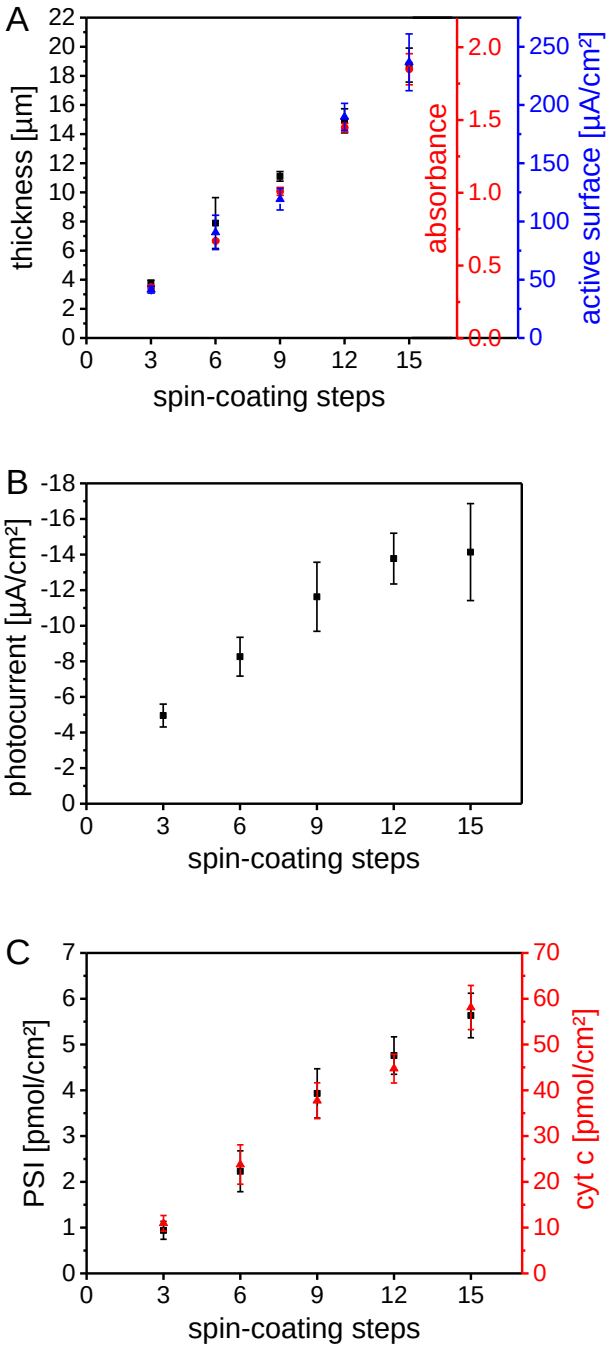

Figure 6. Measurements of electrodes and photobioelectrodes made with 3 to 15 spin-coating steps. Error bars represent the standard deviation of at least 3 measurements. (A) Characterization

of the electrodes: thickness (black squares; SEM), absorbance of the 3D rGO structure in air (red dots; UV/VIS), and electrochemically active surface (blue triangles; cyclic voltammetry in 5 mM PPB pH 7, 100 mV/s); (B) measurements of the photocurrent at -0.15V vs. Ag/AgCl; (C) PSI (black squares) and cyt *c* (red triangles) coverage (PSI amount determined by UV/VIS spectroscopy and cyt *c* coverage by cyclic voltammetry, both described in detail in chapter 2.6).

3.6. Characterization of the Photobioelectrodes

A final test series has been conducted to characterize the photoelectrochemical behavior of the developed electrode prepared from 12 spin coating steps. The stability of the photocurrent is an important aspect of biophotovoltaics. For the evaluation of this facet, photobioelectrodes have been repeatedly illuminated at rather high light intensity (100 mW/cm²) for a total period of 40 min. Additionally, it has been tested how the storage of the PSI electrodes influences the photocurrent output for four days. In between the measurements, the electrodes were stored at 4 °C. There is a decrease in the photo signals with time, however, this decline is only pronounced in the first period of the experiment and slows down during the repeated illumination time. Furthermore, it seems that there is no further degradation within the storage period of the electrode. Figure 7A is an example of a measurement taken after 3 days. Here, only a small decline in photocurrent is visible. From day 3 onwards more than 70 % of the signal of the light pulses can be retained for 40 min.

Next, electrodes have been studied for the influence of the light intensity used for excitation. Thus, illuminations from 0.1 to 100 mW/cm² have been applied. Figure 7B exemplifies that the novel biophotovoltaic system already works well for extremely low intensities producing 1.39 ± 0.15 µA/cm² which is close to 10 % of the maximum output at just 1 ‰ of the intensity.

Additionally, photo action spectroscopy has been performed to analyze the wavelength-depended photocurrent generation of the photobioelectrode. Figure 7C reveals that there is a strong influence of the light energy on the performance of the electrode. Maxima in photocurrent at about 450 nm as well as just below 700 nm indicate that PSI causes the production of photocurrent. Furthermore, control measurements of 3D rGO electrodes incubated with cyt *c* but without PSI demonstrate that there is no detectable photocurrent (see Figure S4). This proves that indeed a photobioelectrode has been developed with PSI as the vital component for electrical power generation.

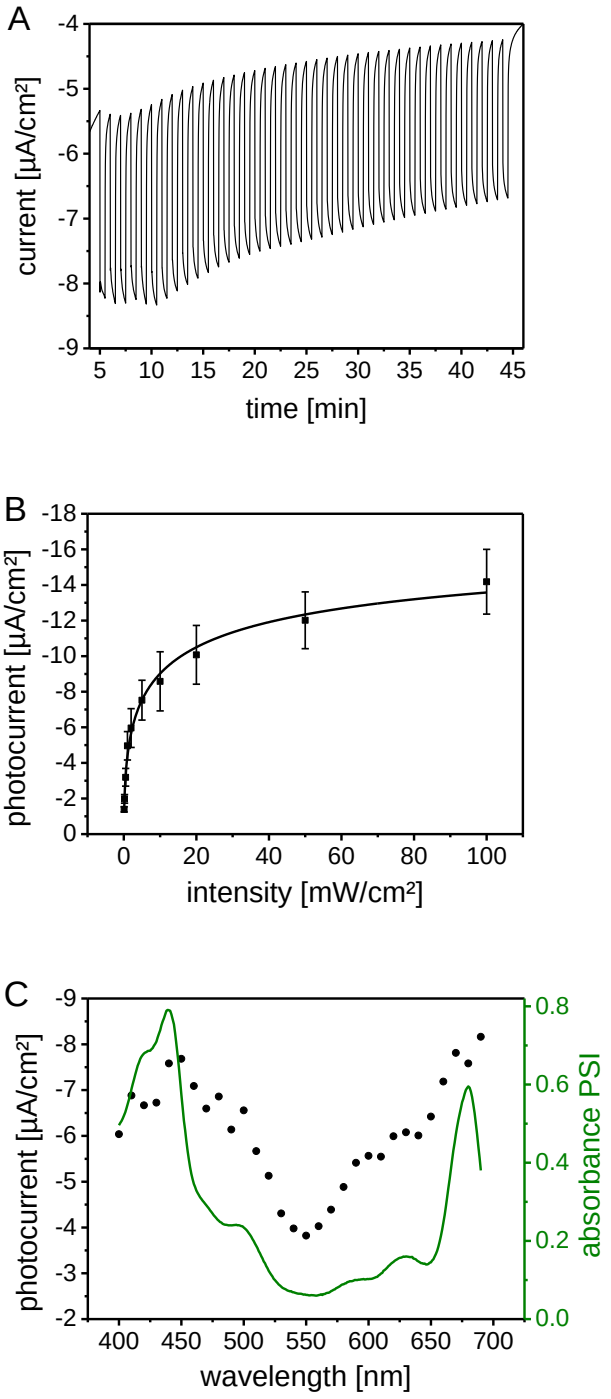

Figure 7. Photocurrent behavior for a photobioelectrode made with 12 spin-coating steps. (A) Example of the long-term stability of photocurrent shown for day 3; (B) Dependence of the photocurrent on illumination intensity. Error bars represent the standard deviation of 3

measurements; (C) photo action spectroscopy by measuring the wavelength dependence of the photocurrent (black squares). For comparison, the UV/VIS absorbance spectrum of a PSI solution in 5 mM PPB pH 7 is added (green line).

With this new photobioelectrode, turnover frequencies (TOF) of 30 e^- PSI^{-1} s^{-1} were achieved at an illumination of 100 mW/cm². External quantum efficiencies (EQE) were 0.07 % under these conditions. The EQE is increasing for lower illuminations up to a value of 6.8 % at 0.1 mW/cm².

As stated in the introduction, this is the first 3D setup combining rGO and PSI which is why no comparative values are available. However, parameters for other biophotovoltaics based on carbon materials can be used for comparison.

There are several 2D approaches known in literature combining carbon surfaces and PSI. They often use graphene, [28,29,35,67] or rGO [33] as artificial electrode material. The graphene-based photobioelectrodes by Feifel et al. provide much higher currents, however, high overpotentials must be applied in this case reducing the obtained power output considerably. [28,29] The biophotovoltaics by Kiliszek et al. yielded significantly lower photocurrents, a maximum of 370 nA/cm² at an overpotential of -300 mV. [35] Nishiori et al. also achieved much lower photoresponses of up to 827 nA/cm² when combining graphene and PSI with the help of gold nanoparticles. As the PSI coverage was determined to be 0.18 pmol/cm², this photoresponse corresponds to a TOF of 47 e^- PSI^{-1} s^{-1}. [67] This number is comparable to the value obtained here. The planar rGO biophotovoltaic described in literature yields three times lower photocurrents at slightly higher potentials. [33]

Bacterial reaction centers have been combined with multi-layer rGO. Here, Csiki et al. used aminomethylferrocene and ubiquinone Q_0 as mediators. A maximum photocurrent of 2.7 µA/cm²

was achieved which is about five times lower than for the photobioelectrode at hand at comparable applied potentials [17].

By comparing this 3D electrode to a system combining PSI and multi-walled carbon nanotubes, it can be noted that comparable photocurrents have been obtained (18 vs. 14 µA/cm²) [32]. Yet, concerning the onset potential, the novel 3D rGO biophotovoltaic surpasses the performance of this electrode by about 150 mV.

When comparing the novel 3D rGO-PSI photobioelectrode to a fullerene-based one, similar results for the onset potential have been found [47]. The photocurrent magnitude is comparable, but one must note here that the latter used a significantly more negative overpotential during photocurrent measurements (-325 vs. -150 mV vs. Ag/AgCl/3M KCl).

As stated in the introduction, a biophotovoltaic system combining 3D rGO and PSII has already been reported [14]. This setup yielded 12.31 µA/cm² at thicknesses of the 3D material of about 20 µm. The novel PSI photobioelectrode at hand surpasses that photoresponse slightly by 15%. When the TOF from that system is evaluated from the photocurrent measurement (and not from oxygen conversion as in the publication), then also here comparable values are obtained in relation to the present report (25 vs. 30 $e^- PSI^{-1} s^{-1}$).

Finally, it should be noted, that for none of the comparable photobioelectrodes described in literature such significant photocurrent production at extremely low illumination intensity has been reported. Photosignals have been obtained down to illuminations with 0.1 mW/cm². EQE of 6.8 % has been achieved under these conditions.

4. Conclusion

A three-dimensional electrode structure of reduced graphene oxide (rGO) has been constructed and linked with photosystem I (PSI) to form a novel biophotovoltaic system.

For the preparation of this electrode type, a template approach using latex beads and graphene oxide has been combined with a spin-coating process. The so prepared 3D graphene oxide is reduced by a chemical treatment with hydrazine.

After characterizing the electrode material first different immobilization strategies of PSI are evaluated. Short incubation times with rather high protein concentrations proved to be beneficial. It can be shown that direct electron transfer to the supercomplex PSI is possible at this 3D electrode structure. The photocurrent generation can be increased by more than one order of magnitude by mediated electron transfer via co-immobilized cytochrome *c* (cyt *c*). Further modification of the surface by bipyridine and adjusting the immobilization protocol for PSI and cyt *c* result in a reproducible photobioelectrode system.

Scalability is an important feature of 3D biophotovoltaics. Electrodes prepared with different numbers of deposition steps and thus, thicknesses (ranging ca. from 4 µm to 19 µm) have been manufactured. Structural and electrochemical analysis demonstrate the gain in the electroactive surface area with increasing thickness while retaining transparency to a certain extent up to 12 spin-coated layers (15µm).

Photobioelectrodes with immobilized PSI and cyt *c* show that the photoresponse can be linearly enhanced up to 12 deposition steps during preparation. For such a 12-layer electrode, the maximum photocurrent at a potential of -0.15 V vs Ag/AgCl and illumination by 100 mW/cm² is 13.7 ± 1.4 µA/cm². This photocurrent and the protein coverage correspond to a turnover frequency of 30 e^- PSI^{-1} s^{-1} and external quantum efficiency (EQE) of 0.07 %. Limitations seem to be mainly caused by reduced transmission at higher electrode thicknesses. The developed photobioelectrode

can be used for several days in solution. It already shows photocurrent generation at low light intensities down to 0.1 mW/cm². EQE of 6.8 % has been achieved under these conditions.

There are multiple starting points on how this novel biophotovoltaic electrode can be further improved. As transparency seems to be an issue that hinders the photocurrent to increase for thicker electrode structures – although protein penetration can be ensured – one possibility can be recognized in the preparation of structures with thinner walls. Further points of optimization can be seen in the size of the used template (latex beads). A different aspect is related to substances and processes which effectively take the photogenerated electrons at the stromal side (faster than oxygen used here in this study). [29,32,47]

Supporting Information

Supporting information is available at the publisher's website free of charge and contains: Intensity spectrum of the light source for photo measurements, chopped-light voltammetry for two electrodes with and without surface modification, photocurrent and standard deviation for two different incubation processes, and photocurrent measurement of an electrode without PSI as a negative control.

Corresponding authors

Sascha Morlock: Tel: +49 3375/508-221. E-mail: sascha.morlock@th-wildau.de

Fred Lisdat: Tel: +49 3375/508-456. E-mail: flisdat@th-wildau.de

Authors' contribution

S. M. and F. L. designed research; S. M. and S. K. S. performed research; S. M. and F. L. analyzed and discussed data; S. M. prepared the figures; S. M. drafted the paper; the manuscript was written through contributions of all authors. All authors approve the final version of the manuscript.

Conflict of interest/Competing interests

The authors declare no conflicts of interest.

Acknowledgments

Financial support by the Federal Ministry for Education and Research (BMBF) within the project 031B0557A+B (Biotechnology 2020) is highly acknowledged. The authors thank J. Wersig, and G. Bartels for excellent technical assistance, funded by the German Research Foundation (DFG) via the Collaborative Research Center SFB 1078 (Project A5, Zouni/Dobbek) and Germany´s Excellence Strategy (Project EXC 2008/1-390540038), respectively.

Abbreviations

rGO, reduced graphene oxide; GO, graphene oxide; PSI, photosystem I; PSII, photosystem II; cyt *c*, cytochrome *c*; EQE, external quantum efficiency; TOF, turnover frequency; SHE, standard hydrogen electrode; DET, direct electron transfer; MET, mediated electron transfer; ITO, indium tin oxide; FTO, fluorine-doped tin oxide; GCE, glasslike carbon electrode chips; PPB, potassium phosphate buffer; LB, latex beads; bipy, 4,4’-bipyridine; CV, cyclic voltammogram; SEM, scanning electron microscopy.

References

(1) Crowe, S. A.; Døssing, L. N.; Beukes, N. J.; Bau, M.; Kruger, S. J.; Frei, R.; Canfield, D. E. Atmospheric oxygenation three billion years ago. *Nature* **2013**, *501* (7468), 535–538. DOI: 10.1038/nature12426.

(2) Zouni, A.; Jordan, R.; Schlodder, E.; Fromme, P.; Witt, H. T. First photosystem II crystals capable of water oxidation. *Biochimica et Biophysica Acta (BBA) - Bioenergetics* **2000**, *1457* (3), 103–105. DOI: 10.1016/S0005-2728(00)00100-6.

(3) Janssen, G. J.; Bielytskyi, P.; Artiukhin, D. G.; Neugebauer, J.; Groot, H. J. M. de; Matysik, J.; Alia, A. Photochemically induced dynamic nuclear polarization NMR on photosystem II: donor cofactor observed in entire plant. *Scientific reports* **2018**, *8* (1), 17853. DOI: 10.1038/s41598-018-36074-z.

(4) Witt, H. T. Primary reactions of oxygenic photosynthesis. *Berichte der Bunsengesellschaft für physikalische Chemie* **1996**, *100* (12), 1923–1942. DOI: 10.1002/bbpc.19961001202.

(5) Teodor, A. H.; Bruce, B. D. Putting Photosystem I to Work: Truly Green Energy. *Trends in biotechnology* **2020.** DOI: 10.1016/j.tibtech.2020.04.004.

(6) Krieger-Liszkay, A.; Fufezan, C.; Trebst, A. Singlet oxygen production in photosystem II and related protection mechanism. *Photosynthesis research* **2008**, *98* (1-3), 551–564. DOI: 10.1007/s11120-008-9349-3.

(7) Vass, I. Molecular mechanisms of photodamage in the Photosystem II complex. *Biochimica et biophysica acta* **2012**, *1817* (1), 209–217. DOI: 10.1016/j.bbabio.2011.04.014.

(8) Passantino, J. M.; Wolfe, K. D.; Simon, K. T.; Cliffel, D. E.; Jennings, G. K. Photosystem I Enhances the Efficiency of a Natural, Gel-Based Dye-Sensitized Solar Cell. *ACS Appl. Bio Mater.* **2020**, *3* (7), 4465–4473. DOI: 10.1021/acsabm.0c00446.

(9) Feifel, S. C.; Stieger, K. R.; Hejazi, M.; Wang, X.; Ilbert, M.; Zouni, A.; Lojou, E.; Lisdat, F. Dihemic c4-type cytochrome acting as a surrogate electron conduit: Artificially interconnecting a photosystem I supercomplex with electrodes. *Electrochemistry Communications* **2018**, *91*, 49–53. DOI: 10.1016/j.elecom.2018.05.006.

(10) Stieger, K. R.; Feifel, S. C.; Lokstein, H.; Hejazi, M.; Zouni, A.; Lisdat, F. Biohybrid architectures for efficient light-to-current conversion based on photosystem I within scalable 3D mesoporous electrodes. *J. Mater. Chem. A* **2016**, *4* (43), 17009–17017. DOI: 10.1039/C6TA07141D.

(11) Faulkner, C. J.; Lees, S.; Ciesielski, P. N.; Cliffel, D. E.; Jennings, G. K. Rapid assembly of photosystem I monolayers on gold electrodes. *Langmuir : the ACS journal of surfaces and colloids* **2008**, *24* (16), 8409–8412. DOI: 10.1021/la800670b.

(12) Riedel, M.; Wersig, J.; Ruff, A.; Schuhmann, W.; Zouni, A.; Lisdat, F. A Z-Scheme-Inspired Photobioelectrochemical H 2 O/O 2 Cell with a 1 V Open-Circuit Voltage Combining Photosystem II and PbS Quantum Dots. *Angew. Chem.* **2018.** DOI: 10.1002/ange.201811172.

(13) Wang, P.; Zhao, F.; Hartmann, V.; Nowaczyk, M. M.; Ruff, A.; Schuhmann, W.; Conzuelo, F. Reassessing the rationale behind herbicide biosensors: The case of a photosystem II/redox polymer-based bioelectrode. *Bioelectrochemistry (Amsterdam, Netherlands)* **2020**, *136*, 107597. DOI: 10.1016/j.bioelechem.2020.107597.

(14) Fang, X.; Sokol, K. P.; Heidary, N.; Kandiel, T. A.; Zhang, J. Z.; Reisner, E. Structure-Activity Relationships of Hierarchical Three-Dimensional Electrodes with Photosystem II for

Semiartificial Photosynthesis. *Nano letters* **2019**, *19* (3), 1844–1850. DOI: 10.1021/acs.nanolett.8b04935.
(15) Katz, E. Application of bifunctional reagents for immobilization of proteins on a carbon electrode surface: Oriented immobilization of photosynthetic reaction centers. *Journal of Electroanalytical Chemistry* **1994**, *365* (1-2), 157–164. DOI: 10.1016/0022-0728(93)02975-N.
(16) Grattieri, M.; Patterson, S.; Copeland, J.; Klunder, K.; Minteer, S. D. Purple Bacteria and 3D Redox Hydrogels for Bioinspired Photo-bioelectrocatalysis. *ChemSusChem* **2020**, *13* (1), 230–237. DOI: 10.1002/cssc.201902116.
(17) Csiki, R.; Drieschner, S.; Lyuleeva, A.; Cattani-Scholz, A.; Stutzmann, M.; Garrido, J. A. Photocurrent generation of biohybrid systems based on bacterial reaction centers and graphene electrodes. *Diamond and Related Materials* **2018**, *89*, 286–292. DOI: 10.1016/j.diamond.2018.09.005.
(18) Pankratova, G.; Pankratov, D.; Di Bari, C.; Goñi-Urtiaga, A.; Toscano, M. D.; Chi, Q.; Pita, M.; Lo Gorton; Lacey, A. L. de. Three-Dimensional Graphene Matrix-Supported and Thylakoid Membrane-Based High-Performance Bioelectrochemical Solar Cell. *ACS Appl. Energy Mater.* **2018**, *1* (2), 319–323. DOI: 10.1021/acsaem.7b00249.
(19) Rasmussen, M.; Wingersky, A.; Minteer, S. D. Comparative study of thylakoids from higher plants for solar energy conversion and herbicide detection. *Electrochimica Acta* **2014**, *140*, 304–308. DOI: 10.1016/j.electacta.2014.02.121.
(20) Masi, M.; Bollella, P.; Riedel, M.; Lisdat, F.; Katz, E. Photobiofuel Cell with Sustainable Energy Generation Based on Micro/Nanostructured Electrode Materials. *ACS Appl. Energy Mater.* **2020**, *3* (10), 9543–9549. DOI: 10.1021/acsaem.0c02169.
(21) Dumas, C.; Mollica, A.; Féron, D.; Basséguy, R.; Etcheverry, L.; Bergel, A. Marine microbial fuel cell: Use of stainless steel electrodes as anode and cathode materials. *Electrochimica Acta* **2007**, *53* (2), 468–473. DOI: 10.1016/j.electacta.2007.06.069.
(22) Ciniciato, G. P. M. K.; Ng, F.-L.; Phang, S.-M.; Jaafar, M. M.; Fisher, A. C.; Yunus, K.; Periasamy, V. Investigating the association between photosynthetic efficiency and generation of biophotoelectricity in autotrophic microbial fuel cells. *Scientific reports* **2016**, *6*, 31193. DOI: 10.1038/srep31193.
(23) Bombelli, P.; Zarrouati, M.; Thorne, R. J.; Schneider, K.; Rowden, S. J. L.; Ali, A.; Yunus, K.; Cameron, P. J.; Fisher, A. C.; Ian Wilson, D.; Howe, C. J.; McCormick, A. J. Surface morphology and surface energy of anode materials influence power outputs in a multi-channel mediatorless bio-photovoltaic (BPV) system. *Physical chemistry chemical physics : PCCP* **2012**, *14* (35), 12221–12229. DOI: 10.1039/c2cp42526b.
(24) Tapia, C.; Milton, R. D.; Pankratova, G.; Minteer, S. D.; Åkerlund, H.-E.; Leech, D.; De Lacey, A. L.; Pita, M.; Lo Gorton. Wiring of Photosystem I and Hydrogenase on an Electrode for Photoelectrochemical H 2 Production by using Redox Polymers for Relatively Positive Onset Potential. *ChemElectroChem* **2017**, *4* (1), 90–95. DOI: 10.1002/celc.201600506.
(25) Sokol, K. P.; Robinson, W. E.; Warnan, J.; Kornienko, N.; Nowaczyk, M. M.; Ruff, A.; Zhang, J. Z.; Reisner, E. Bias-free photoelectrochemical water splitting with photosystem II on a dye-sensitized photoanode wired to hydrogenase. *Nat Energy* **2018**, *3* (11), 944–951. DOI: 10.1038/s41560-018-0232-y.

(26) Ciornii, D.; Riedel, M.; Stieger, K. R.; Feifel, S. C.; Hejazi, M.; Lokstein, H.; Zouni, A.; Lisdat, F. Bioelectronic Circuit on a 3D Electrode Architecture: Enzymatic Catalysis Interconnected with Photosystem I. *Journal of the American Chemical Society* **2017**, *139* (46), 16478–16481. DOI: 10.1021/jacs.7b10161.
(27) Habermüller, K.; Mosbach, M.; Schuhmann, W. Electron-transfer mechanisms in amperometric biosensors. *Fresenius' journal of analytical chemistry* **2000**, *366* (6-7), 560–568. DOI: 10.1007/s002160051551.
(28) Feifel, S. C.; Lokstein, H.; Hejazi, M.; Zouni, A.; Lisdat, F. Unidirectional Photocurrent of Photosystem I on π-System-Modified Graphene Electrodes: Nanobionic Approaches for the Construction of Photobiohybrid Systems. *Langmuir : the ACS journal of surfaces and colloids* **2015**, *31* (38), 10590–10598. DOI: 10.1021/acs.langmuir.5b01625.
(29) Feifel, S. C.; Stieger, K. R.; Lokstein, H.; Lux, H.; Lisdat, F. High photocurrent generation by photosystem I on artificial interfaces composed of π-system-modified graphene. *J. Mater. Chem. A* **2015**, *3* (23), 12188–12196. DOI: 10.1039/C5TA00656B.
(30) Yehezkeli, O.; Tel-Vered, R.; Michaeli, D.; Nechushtai, R.; Willner, I. Photosystem I (PSI)/Photosystem II (PSII)-based photo-bioelectrochemical cells revealing directional generation of photocurrents. *Small (Weinheim an der Bergstrasse, Germany)* **2013**, *9* (17), 2970–2978. DOI: 10.1002/smll.201300051.
(31) Gizzie, E. A.; LeBlanc, G.; Jennings, G. K.; Cliffel, D. E. Electrochemical preparation of Photosystem I-polyaniline composite films for biohybrid solar energy conversion. *ACS applied materials & interfaces* **2015**, *7* (18), 9328–9335. DOI: 10.1021/acsami.5b01065.
(32) Ciornii, D.; Feifel, S. C.; Hejazi, M.; Kölsch, A.; Lokstein, H.; Zouni, A.; Lisdat, F. Construction of photobiocathodes using multi-walled carbon nanotubes and photosystem I. *Phys. Status Solidi A* **2017**, *214* (9), 1700017. DOI: 10.1002/pssa.201700017.
(33) Darby, E.; LeBlanc, G.; Gizzie, E. A.; Winter, K. M.; Jennings, G. K.; Cliffel, D. E. Photoactive films of photosystem I on transparent reduced graphene oxide electrodes. *Langmuir : the ACS journal of surfaces and colloids* **2014**, *30* (29), 8990–8994. DOI: 10.1021/la5010616.
(34) Ciornii, D.; Kölsch, A.; Zouni, A.; Lisdat, F. A precursor-approach in constructing 3D ITO electrodes for the improved performance of photosystem I-cyt c photobioelectrodes. *Nanoscale* **2019**, *11* (34), 15862–15870. DOI: 10.1039/c9nr04344f.
(35) Kiliszek, M.; Harputlu, E.; Szalkowski, M.; Kowalska, D.; Unlu, C. G.; Haniewicz, P.; Abram, M.; Wiwatowski, K.; Niedziółka-Jönsson, J.; Maćkowski, S.; Ocakoglu, K.; Kargul, J. Orientation of photosystem I on graphene through cytochrome c553 leads to improvement in photocurrent generation. *J. Mater. Chem. A* **2018**, *6* (38), 18615–18626. DOI: 10.1039/C8TA02420K.
(36) Wolfe, K. D.; Dervishogullari, D.; Passantino, J. M.; Stachurski, C. D.; Jennings, G. K.; Cliffel, D. E. Improving the stability of photosystem I–based bioelectrodes for solar energy conversion. *Current Opinion in Electrochemistry* **2020**, *19*, 27–34. DOI: 10.1016/j.coelec.2019.09.009.
(37) Stieger, K. R.; Feifel, S. C.; Lokstein, H.; Lisdat, F. Advanced unidirectional photocurrent generation via cytochrome c as reaction partner for directed assembly of photosystem I. *Physical chemistry chemical physics : PCCP* **2014**, *16* (29), 15667–15674. DOI: 10.1039/c4cp00935e.

(38) Ciesielski, P. N.; Faulkner, C. J.; Irwin, M. T.; Gregory, J. M.; Tolk, N. H.; Cliffel, D. E.; Jennings, G. K. Enhanced Photocurrent Production by Photosystem I Multilayer Assemblies. *Adv. Funct. Mater.* **2010**, *20* (23), 4048–4054. DOI: 10.1002/adfm.201001193.
(39) Stieger, K. R.; Ciornii, D.; Kölsch, A.; Hejazi, M.; Lokstein, H.; Feifel, S. C.; Zouni, A.; Lisdat, F. Engineering of supramolecular photoactive protein architectures: the defined co-assembly of photosystem I and cytochrome c using a nanoscaled DNA-matrix. *Nanoscale* **2016**, *8* (20), 10695–10705. DOI: 10.1039/c6nr00097e.
(40) Badura, A.; Guschin, D.; Kothe, T.; Kopczak, M. J.; Schuhmann, W.; Rögner, M. Photocurrent generation by photosystem 1 integrated in crosslinked redox hydrogels. *Energy Environ. Sci.* **2011**, *4* (7), 2435. DOI: 10.1039/c1ee01126j.
(41) Zhao, F.; Plumeré, N.; Nowaczyk, M. M.; Ruff, A.; Schuhmann, W.; Conzuelo, F. Interrogation of a PS1-Based Photocathode by Means of Scanning Photoelectrochemical Microscopy. *Small (Weinheim an der Bergstrasse, Germany)* **2017**, *13* (26). DOI: 10.1002/smll.201604093.
(42) Mersch, D.; Lee, C.-Y.; Zhang, J. Z.; Brinkert, K.; Fontecilla-Camps, J. C.; Rutherford, A. W.; Reisner, E. Wiring of Photosystem II to Hydrogenase for Photoelectrochemical Water Splitting. *Journal of the American Chemical Society* **2015**, *137* (26), 8541–8549. DOI: 10.1021/jacs.5b03737.
(43) Manocchi, A. K.; Baker, D. R.; Pendley, S. S.; Nguyen, K.; Hurley, M. M.; Bruce, B. D.; Sumner, J. J.; Lundgren, C. A. Photocurrent generation from surface assembled photosystem I on alkanethiol modified electrodes. *Langmuir : the ACS journal of surfaces and colloids* **2013**, *29* (7), 2412–2419. DOI: 10.1021/la304477u.
(44) Peters, K.; Lokupitiya, H. N.; Sarauli, D.; Labs, M.; Pribil, M.; Rathouský, J.; Kuhn, A.; Leister, D.; Stefik, M.; Fattakhova-Rohlfing, D. Nanostructured Antimony-Doped Tin Oxide Layers with Tunable Pore Architectures as Versatile Transparent Current Collectors for Biophotovoltaics. *Adv. Funct. Mater.* **2016**, *26* (37), 6682–6692. DOI: 10.1002/adfm.201602148.
(45) Kondo, M.; Amano, M.; Joke, T.; Ishigure, S.; Noji, T.; Dewa, T.; Amao, Y.; Nango, M. Immobilization of photosystem I or II complexes on electrodes for preparation of photoenergy-conversion devices. *Res Chem Intermed* **2014**, *40* (9), 3287–3293. DOI: 10.1007/s11164-014-1833-0.
(46) Mershin, A.; Matsumoto, K.; Kaiser, L.; Yu, D.; Vaughn, M.; Nazeeruddin, M. K.; Bruce, B. D.; Graetzel, M.; Zhang, S. Self-assembled photosystem-I biophotovoltaics on nanostructured TiO(2)and ZnO. *Scientific reports* **2012**, *2*, 234. DOI: 10.1038/srep00234.
(47) Ciornii, D.; Kölsch, A.; Zouni, A.; Lisdat, F. Exploiting new ways for a more efficient orientation and wiring of PSI to electrodes: A fullerene C70 approach. *Electrochimica Acta* **2019**, *299*, 531–539. DOI: 10.1016/j.electacta.2019.01.032.
(48) Gunther, D.; LeBlanc, G.; Prasai, D.; Zhang, J. R.; Cliffel, D. E.; Bolotin, K. I.; Jennings, G. K. Photosystem I on graphene as a highly transparent, photoactive electrode. *Langmuir : the ACS journal of surfaces and colloids* **2013**, *29* (13), 4177–4180. DOI: 10.1021/la305020c.
(49) Chen, J.-H.; Jang, C.; Xiao, S.; Ishigami, M.; Fuhrer, M. S. Intrinsic and extrinsic performance limits of graphene devices on SiO2. *Nature nanotechnology* **2008**, *3* (4), 206–209. DOI: 10.1038/nnano.2008.58.

(50) Lee, C.; Wei, X.; Kysar, J. W.; Hone, J. Measurement of the elastic properties and intrinsic strength of monolayer graphene. *Science (New York, N.Y.)* **2008**, *321* (5887), 385–388. DOI: 10.1126/science.1157996.
(51) Novoselov, K. S.; Geim, A. K.; Morozov, S. V.; Jiang, D.; Zhang, Y.; Dubonos, S. V.; Grigorieva, I. V.; Firsov, A. A. Electric field effect in atomically thin carbon films. *Science (New York, N.Y.)* **2004**, *306* (5696), 666–669. DOI: 10.1126/science.1102896.
(52) Xu, Y.; Cao, H.; Xue, Y.; Li, B.; Cai, W. Liquid-Phase Exfoliation of Graphene: An Overview on Exfoliation Media, Techniques, and Challenges. *Nanomaterials (Basel, Switzerland)* **2018**, *8* (11). DOI: 10.3390/nano8110942.
(53) Bao, J.; Norimatsu, W.; Iwata, H.; Matsuda, K.; Ito, T.; Kusunoki, M. Synthesis of Freestanding Graphene on SiC by a Rapid-Cooling Technique. *Physical review letters* **2016**, *117* (20), 205501. DOI: 10.1103/PhysRevLett.117.205501.
(54) Phiri, J.; Gane, P.; Maloney, T. C. General overview of graphene: Production, properties and application in polymer composites. *Materials Science and Engineering: B* **2017**, *215*, 9–28. DOI: 10.1016/j.mseb.2016.10.004.
(55) Toh, S. Y.; Loh, K. S.; Kamarudin, S. K.; Daud, W. R. W. Graphene production via electrochemical reduction of graphene oxide: Synthesis and characterisation. *Chemical Engineering Journal* **2014**, *251*, 422–434. DOI: 10.1016/j.cej.2014.04.004.
(56) Silva, K. K. H. de; Huang, H.-H.; Joshi, R.; Yoshimura, M. Restoration of the graphitic structure by defect repair during the thermal reduction of graphene oxide. *Carbon* **2020**, *166*, 74–90. DOI: 10.1016/j.carbon.2020.05.015.
(57) Silva, K.K.H. de; Huang, H.-H.; Joshi, R. K.; Yoshimura, M. Chemical reduction of graphene oxide using green reductants. *Carbon* **2017**, *119*, 190–199. DOI: 10.1016/j.carbon.2017.04.025.
(58) Wu, Y.; Zhu, J.; Huang, L. A review of three-dimensional graphene-based materials: Synthesis and applications to energy conversion/storage and environment. *Carbon* **2019**, *143*, 610–640. DOI: 10.1016/j.carbon.2018.11.053.
(59) Kern, J.; Loll, B.; Lüneberg, C.; DiFiore, D.; Biesiadka, J.; Irrgang, K.-D.; Zouni, A. Purification, characterisation and crystallisation of photosystem II from Thermosynechococcus elongatus cultivated in a new type of photobioreactor. *Biochimica et biophysica acta* **2005**, *1706* (1-2), 147–157. DOI: 10.1016/j.bbabio.2004.10.007.
(60) Kölsch, A.; Hejazi, M.; Stieger, K. R.; Feifel, S. C.; Kern, J. F.; Müh, F.; Lisdat, F.; Lokstein, H.; Zouni, A. Insights into the binding behavior of native and non-native cytochromes to photosystem I from Thermosynechococcus elongatus. *The Journal of biological chemistry* **2018**, *293* (23), 9090–9100. DOI: 10.1074/jbc.RA117.000953.
(61) Müh, F.; Zouni, A. Extinction coefficients and critical solubilisation concentrations of photosystems I and II from Thermosynechococcus elongatus. *Biochimica et biophysica acta* **2005**, *1708* (2), 219–228. DOI: 10.1016/j.bbabio.2005.03.005.
(62) Golub, M.; Hejazi, M.; Kölsch, A.; Lokstein, H.; Wieland, D. C. F.; Zouni, A.; Pieper, J. Solution structure of monomeric and trimeric photosystem I of Thermosynechococcus elongatus investigated by small-angle X-ray scattering. *Photosynth Res* **2017**, *133* (1-3), 163–173. DOI: 10.1007/s11120-017-0342-6.

(63) Choi, B. G.; Yang, M.; Hong, W. H.; Choi, J. W.; Huh, Y. S. 3D macroporous graphene frameworks for supercapacitors with high energy and power densities. *ACS nano* **2012**, *6* (5), 4020–4028. DOI: 10.1021/nn3003345.
(64) Porra, R. J. A simple method for extracting chlorophylls from the recalcitrant alga, Nannochloris atomus, without formation of spectroscopically-different magnesium-rhodochlorin derivatives. *Biochimica et Biophysica Acta (BBA) - Bioenergetics* **1990**, *1019* (2), 137–141. DOI: 10.1016/0005-2728(90)90135-Q.
(65) Zhang, W.; Zhang, Y.; Tian, Y.; Yang, Z.; Xiao, Q.; Guo, X.; Jing, L.; Zhao, Y.; Yan, Y.; Feng, J.; Sun, K. Insight into the capacitive properties of reduced graphene oxide. *ACS applied materials & interfaces* **2014**, *6* (4), 2248–2254. DOI: 10.1021/am4057562.
(66) Baker, S. E.; Colavita, P. E.; Tse, K.-Y.; Hamers, R. J. Functionalized Vertically Aligned Carbon Nanofibers as Scaffolds for Immobilization and Electrochemical Detection of Redox-Active Proteins. *Chem. Mater.* **2006**, *18* (18), 4415–4422. DOI: 10.1021/cm0609000.
(67) Nishiori, D.; Zhu, W.; Salles, R.; Miyachi, M.; Yamanoi, Y.; Ikuta, T.; Maehashi, K.; Tomo, T.; Nishihara, H. Photosensing System Using Photosystem I and Gold Nanoparticle on Graphene Field-Effect Transistor. *ACS applied materials & interfaces* **2019**, *11* (45), 42773–42779. DOI: 10.1021/acsami.9b14771.

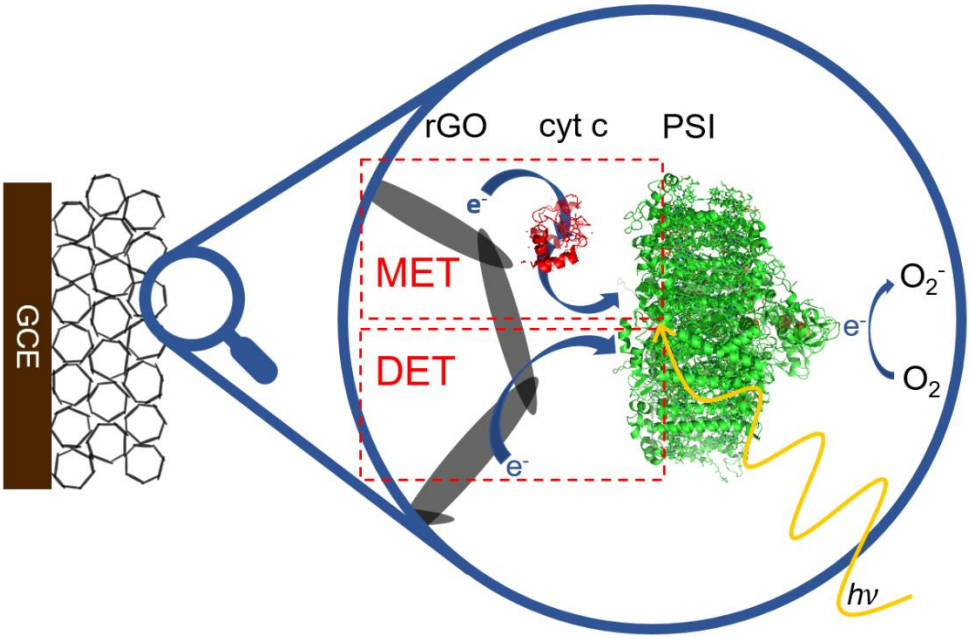
rGO
cyt c
PSI
GCE
MET
DET
e-
e-
e-
O2-
O2
hν